文章编号：1001－9014(2015)05－0520－08

DOI:10.11972/j.issn.1001－9014.2015.05.002

Parametric modelling of the lossy folded waveguide circuits for the 220 GHz backward wave oscillator

CAI Jin-Chi[1,2*], HU Lin-Lin[2], MA Guo-Wu[2], CHEN Hong-Bin[2], JIN Xiao[2], CHEN Huai-Bi[1]

(1. Dept. of Engineering Physics, Tsinghua University, Beijing 100084, China;
2. Institute of Applied Electronics, China Academy of Engineering Physics, Mianyang 621000, China)

Abstract: The equivalent circuit model (ECM) of the folded waveguide (FW) in consistent consideration of the ohm loss on the waveguide wall was established for calculating the cold-circuit phase velocities, interaction impedance and attenuating coefficient of space harmonics of periodic TE_{10} mode in this slow wave structure (SWS). These results were obtained for one-dimensional (1-D) parametric model calculation of the particle-microwave interaction in the 220 GHz backward wave oscillator (BWO). When the frequency of microwave is up to terahertz regime, the ohm loss caused by surface current on rough waveguide wall is not negligible any more. Further study shows that the starting oscillation current and output power are intimately dependent upon the loss property calculation. The ECM about lossy periodic circuits was then developed from the previous loss-free model to give a more accurate analysis. Three-dimensional (3-D) Eigen mode analysis for the FW SWS was taken to verify the improved model, which shows good agreement. Additionally, based on the improved ECM, 1-D beam wave interaction calculation was conducted which is in good consistency with 3-D Particle-in-cell (PIC) method.

Key words: Terahertz, folded waveguide, equivalent circuit model, ohm loss
PACS: 07.50.-e, 07.57.Hm

220 GHz 折叠波导慢波结构的有损参数化模型

蔡金赤[1,2*], 胡林林[2], 马国武[2], 陈洪斌[2], 金 晓[2], 陈怀壁[1]

(1. 清华大学工程物理系, 北京 100084;
2. 中国工程物理研究院应用电子学研究所, 四川 绵阳 621000)

摘要: 建立了自洽的考虑波导壁损耗的折叠波导等效电路模型, 用来计算该慢波结构周期 TE_{10} 模式中各次空间谐波的相速度, 耦合阻抗和线衰减系数. 分析结果将会用到 220 GHz 折叠波导返波管一维束波互作用模型的计算中. 当微波频率上升到太赫兹波段时, 粗糙波导表面电流导致的壁损将不能再忽略不计. 进一步研究表明, 起振电流和输出功率水平将和损耗特性的计算密切相关. 从原有模型发展而来的有损电路模型可以给出更准确损耗估计. 建立了折叠波导慢波线三维谐振腔模型来验证本文的等效电路理论, 有较好的吻合. 采用了该理论导出参数的一维束波互作用模型和三维数值 PIC 方法同样有很好的一致性.

关 键 词: 太赫兹; 折叠波导; 等效电路模型; 欧姆损耗

中图分类号: TN802　　**文献标识码**: A

Introduction

The terahertz science and technology has great application of high speed wireless communication, high resolution imaging, damage-free biochemistry analysis and so on in the near future[1]. As a microwave generator, BWO possesses a desirable power-to-volume ratio, great convenience of frequency-tuned ability and relative low noise, making it a stable standard seed power source in terahertz research area[2]. The advanced plane machining technologies such as LIGA (Lithographie, Galano-

Received date: 2014-05-19, **revised date**: 2015-03-01　　**收稿日期**: 2014-05-19, **修回日期**: 2015-03-01
Foundation items: Supported by preliminary research Foundation of CAEP (426050502-2)
Biography: Cai Jin-Chi (1987-), male, Sichuan, China, PhD. Research fields focus on terahertz technology.
* **Corresponding author**: E-mail: caijinchino1@163.com

formung, Abformung) and DRIE (Deep Reactive Ion Etching) make the FW structure a promising SWS in terahertz regime, which also demonstrates other merits in heat dissipation, power capacity, flat dispersion property, etc[3].

The 220 GHz FW BWO is being developed in the institution of Applied Electronics of China Academy of Engineering Physics (IAE, CAEP). The BWO design comprises of the design of SWS, the beam optical system (BOS), the power coupler and the mechanical design. The 3-D PIC method is a precise tool to impose a judgment on the design scheme. Nevertheless, it is source-consuming and time-consuming in the preliminary optimization process on the basis of the mainstream computer configuration. 1-D beam-wave interaction equations were then derived in our design stage to give a fast parameter design of the SWS shown in Fig. 1.

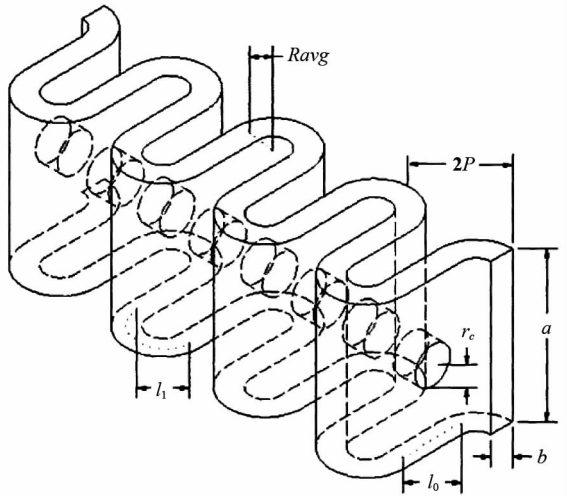

Fig. 1　The schematic of folded waveguide SWS[4]
图 1　叠波导慢波结构示意图[4]

As a significant part of the 1-D model, the axial phase velocity, the interaction impedance and the field attenuation factor of the space harmonics of the periodic TE_{10} mode in the SWS should be offered in analytical methods. For more accurate calculation of the starting oscillation current and output power level of BWO, the consistent equivalent circuit theory in consideration of the ohm loss was developed from the previous theoretical method[5]. In Part 1, the perturbation of the propagation characteristics induced by ohm loss was described in detail. In Part 2, the equivalent circuit theory of the lossy periodic system was demonstrated. In Part 3, the numerical verifications about this method is given.

1　Lossy Wall Estimation

When the frequency increases, the skin depth of microwave on the metallic wall decreases rapidly, thus inducing a large ohm loss on waveguide surface. In terahertz frequency range, the skin depth of copper can be similar to the surface roughness by conventional machining process, which makes an additional credit for the power dissipation on the waveguide wall. This phenomenon can be equivalent to the modification of the conductivity of the wall material, called the effective conductivity. The effective conductivity can be obtained through measuring the $|S_{21}|$ parameter of the straight uniform waveguide, or can be roughly evaluated through Eq. 1[6-8]:

$$\sigma_c = \frac{\sigma}{(1+e^{-(s/h/2)^{1.6}})^2}, s = \sqrt{\frac{2}{\omega\mu_0\sigma}}$$
$$\sigma = \mathrm{Re}\left(\frac{\sigma_0}{1+j\omega\tau}\right) \quad , \quad (1)$$

where σ_0 is the DC conductivity of the wall material, s is the skin depth of microwave in a certain frequency, h is the surface roughness of metallic wall, ω is the angular frequency, τ is the average electron scattering time in Drude model, which is 13 fs for copper. Eq. 1 is suitable well for the situation that s is much larger than h in a good conductor. When s approximates h, the effective conductivity obtained by Eq. 1 is slightly smaller than the value measured by preliminary experiments.

The TE_{10} mode properties of straight rectangular waveguide with the consideration of the lossy wall is discussed in a self-consistent method, which is more strict than perturbation theory[7]. According to the mode-coupling theory, the perturbed TE_{10} mode is comprised of the modes in lossy-free rectangular waveguide, shown as Eq. 2[9]:

$$-\frac{\mathrm{d}V_i}{\mathrm{d}z} = j\beta_i Z_i I_i + \frac{j\omega\mu_0}{k^2}\cdot j\omega\varepsilon_0 \oint_C \hat{v}\cdot h_i E_z \mathrm{d}l$$
$$-\frac{\mathrm{d}I_i}{\mathrm{d}z} = \frac{j\beta_i}{Z_i} V_i + \frac{j\omega\varepsilon_0}{k^2}\oint_C E_v \nabla_t \cdot h_i \mathrm{d}l \quad , \quad (2)$$

where V_i, I_i is the mode voltage and mode current of a certain coupling mode. β_i, Z_i is the phase-shift rate and mode impedance of the unperturbed mode, e_i, h_i is the normalized transverse electric and magnetic field of the mode i, v is the tangential direction of the circumstance of a certain cross section, k is the wave number of microwave.

When the surface power loss is investigated, the tangential component of the E-field emerges on the metallic boundary, shown in Eq. 3[7]:

$$E_z = -H_v R_s(1+j), E_v = H_z R_s(1+j), R_s = \sqrt{\frac{\omega\mu_0}{2\sigma_c}} \quad , \quad (3)$$

where R_s is the surface resistance of the lossy metallic wall, σ_c is the effective conductivity. With the combination of Eq. 2 and Eq. 3, Eq. 4 is obtained in which the transverse magnetic field on the cross section is expressed by unperturbed mode current and normalized magnetic field:

$$-\frac{\mathrm{d}V_i}{\mathrm{d}z} = j\beta_i Z_i I_i - \frac{j\omega\mu_0}{k^2}\cdot j\omega\varepsilon_0 R_s(1+j)\sum_q I_j \oint_C (\hat{v}h_q)(\hat{v}h_i)\mathrm{d}l$$
$$-\frac{\mathrm{d}I_i}{\mathrm{d}z} = \frac{j\beta_i}{Z_i} V_i + \frac{j\omega\varepsilon_0}{k^2}\cdot\frac{R_s(1+j)}{j\omega\mu_0}\sum_q V_j \oint_C \nabla_t \cdot h_q \nabla_t \cdot h_i \mathrm{d}l \quad . \quad (4)$$

For the perturbed TE_{10} mode in straight rectangular waveguide, the main component of coupling modes is the

unperturbed TE_{10} modes in both propagation direction. Therefore other high-order coupling modes is ignored in Eq. 4. The normalized magnetic field, phase-shift rate and mode impedance of TE_{10} mode can be written as Eq. 5:

$$h = \sqrt{\frac{2}{ab}}\sin(\frac{\pi}{a}x)\hat{x},\beta = \sqrt{(\frac{\omega}{c})^2 - (\frac{\pi}{a})^2}$$
$$Z = \frac{\omega\mu_0}{\beta} \quad , \quad (5)$$

where a is the length of broad side of rectangular waveguide which positioned in the region of $x = [0,a]$, b is the length of narrow side of rectangular waveguide, c is light speed in vacuum. Combining Eq. 4 and Eq. 5, the perturbed TE_{10} mode in consideration of lossy wall possesses the modified phase-shift rate and mode impedance, demonstrated as Eq. 6:

$$\beta_{loss}^2 = \beta^2 - \frac{4R_s^2}{\eta_0^2 b^2}(1+j)^2\frac{k_c^2}{k^2}(1+\frac{2b}{a}) + \frac{2R_s(1+j)k}{j\eta_0 b}(1+\frac{2b}{a}\frac{k_c^2}{k^2})$$
$$Z_{loss}^2 = \frac{j\beta Z + R_s(1+j)\frac{2}{b}}{\frac{j\beta}{Z} + \frac{R_s(1+j)}{\eta_0^2 k^2}\frac{2\pi^2}{a^3 b}(a+2b)} \quad , \quad (6)$$

where β_{loss}, Z_{loss} is the perturbed phase-shift rate and mode impedance, η_0 is wave impedance of TEM wave, k_c is the cut-off wave number of unperturbed TE_{10} mode, equaling to π/a. It is apparent that near-cut-off case and cut-off case can also be discussed based on Eq. 6, where β is a negative imaginary number. Eq. 6 is simplified as Eq. 7 by linear approximation:

$$\beta_{loss} = \beta - j\frac{R_s}{\eta_0}(1+\frac{2b}{a}\frac{k_c^2}{k^2})\frac{1}{b}\frac{k}{\beta}$$
$$Z_{loss} = \frac{\omega\mu_0}{\beta_{loss}} - \frac{2jR_s}{\beta_{loss}b} \quad . \quad (7)$$

The imagine part of β_{loss} is the attenuation coefficient of the attenuating TE_{10} mode. The imagine part of Z_{loss} means the transverse E-field and H-field are no longer synchronized. For loss-free bended waveguide, the phase-shift rate and mode impedance could also be calculated through mode-coupling theory, shown as Eq. 8[10]:

$$\beta' = \frac{\beta}{1+\frac{1}{12}(\frac{b}{R_{avg}})^2[\frac{1}{2} - \frac{1}{5}(b\beta)^2]}$$
$$Z' = Z\{1+\frac{1}{12}(\frac{b}{R_{avg}})^2[\frac{1}{2} - \frac{1}{5}(b\beta)^2]\} \quad , \quad (8)$$

where R_{avg} is the bend radius of bended rectangular waveguide. According to Eq. 8, the mode-coupling equation caused by bend effect is rewritten as Eq. 9:

$$-\frac{dV'}{dz} = j\beta ZI'$$
$$-\frac{dI'}{dz} = \frac{j\beta}{Z}V' + \frac{j\beta}{Z}(\frac{1}{\{1+\frac{1}{12}(\frac{b}{R_{avg}})^2[\frac{1}{2} - \frac{1}{5}(b\beta)^2]\}^2} - 1)V' \quad . \quad (9)$$

Assuming the mode coupling caused by ohm loss and axis bend are independent and can be linearly superposed, the mode voltage and mode current of TE_{10} mode in bend waveguide with lossy wall can be demonstrated as Eq. 10:

$$-\frac{dV'}{dz} = j\beta_{loss}Z_{loss}I'$$
$$-\frac{dI'}{dz} = \frac{j\beta_{loss}}{Z_{loss}}V' + \frac{j\beta}{Z}(\frac{1}{\{1+\frac{1}{12}(\frac{b}{R_{avg}})^2[\frac{1}{2} - \frac{1}{5}(b\beta)^2]\}^2} - 1)V' \quad . \quad (10)$$

Therefore, the phase-shift rate and mode impedance of TE_{10} mode in bended waveguide with the consideration of ohm loss can be derived as Eq. 11, using linear approximation:

$$\beta'_{loss} = \frac{\beta_{loss}}{1+\frac{1}{12}(\frac{b}{R_{avg}})^2[\frac{1}{2} - \frac{1}{5}(b\beta)^2]}$$
$$Z'_{loss} = Z_{loss}\{1+\frac{1}{12}(\frac{b}{R_{avg}})^2[\frac{1}{2} - \frac{1}{5}(b\beta)^2]\} \quad . \quad (11)$$

Equations 7 and 11 will be used to express the transferring matrix of straight rectangular waveguide and bended rectangular waveguide with lossy wall in section three.

2 Equivalent Circuits Model

The periodic TE_{10} mode in the lossy FW SWS was firstly calculated in this Part. A period of the folded waveguide is selected as Fig. 2(a). It should be emphasized that the minimal periodic structure along waveguide serpentine path is the half of the periodic configuration along z direction. It is assumed that the periodic TE_{10} mode includes the TE_{10} mode in straight rectangular waveguide and bended rectangular waveguide, with both propagation direction wave existing. The problem to be solved is to calculate the network transferring matrix of mode voltage and mode current in this SWS composed by beam tunnel section(section A), straight waveguide section (section B), curvature junction section (section BC), bended waveguide section(section C), shown in Fig. 2(b). All the parameters are denoted as in Fig. 1.

The transferring matrix in section B could be written as Eq. 12:

$$\boldsymbol{F_1} = \begin{bmatrix} \cos(\frac{\beta_{loss}l_0}{2}) & -jZ_{loss}\sin(\frac{\beta_{loss}l_0}{2}) \\ -\frac{j}{Z_{loss}}\sin(\frac{\beta_{loss}l_0}{2}) & \cos(\frac{\beta_{loss}l_0}{2}) \end{bmatrix} \quad , (12)$$

where l_0 is the length of the straight rectangular waveguide. The transferring matrix in section C can be written as Eq. 13:

$$\boldsymbol{F_2} = \begin{bmatrix} \cos(\beta'_{loss}l_1) & -jZ_{loss}\sin(\beta_{loss}l_1) \\ -\frac{j}{Z_{loss}}\sin(\beta_{loss}l_1) & \cos(\beta_{loss}l_1) \end{bmatrix} \quad , (13)$$

where l_1 is the length of the bended rectangular waveguide, which equals πp. The transferring matrix of the junction part BC could be written as Eq. 14[4]:

$$\boldsymbol{F_3} = \begin{bmatrix} 1 & jX_1 \\ 0 & 1 \end{bmatrix} \quad . \quad (14)$$

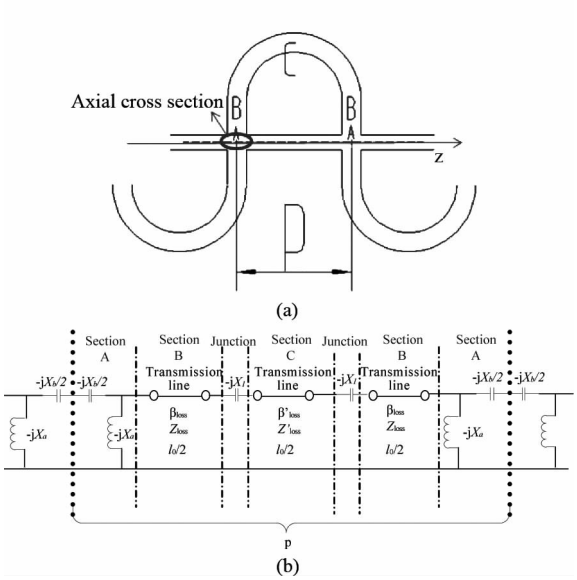

Fig. 2　The FW SWS and its equivalent circuit
图 2　叠波导慢波结构及其等效电路

In section A, X_a and X_b could be written as Eq. 15[5]:

$$\frac{X_b}{Z} = \frac{1}{\frac{ab}{2\beta}\left(\frac{0.4819}{r_c^3} + \frac{\pi}{a^2 b}\right)} \cdot \frac{X_a}{Z} = \frac{1 - \frac{2}{3\pi}\frac{k^2}{b}r_c^3}{\frac{4\beta}{3ab}r_c^3\left(\frac{k}{\beta}\right)^2} \quad ,(15)$$

where r_c is the radius of the round beam tunnel. The beam tunnel induces the discontinuity in the FW SWS, the equivalent circuit is shown in Fig. 2. Strictly speaking, the relative field distribution of TE_{10} mode can be drastically distorted near the beam tunnel aperture. Therefore, the mode impedance of the axial cross section calculated by transferring matrix should be further revised. For periodic phase shift calculation, the equivalent circuit is reasonable.

As an approximation, the waveguide loss has little influence on the mode match in junction part BC and junction part A. The whole transferring matrix of this periodic structure is achieved by multiplying the transferring matrix of each section one by one, demonstrated as Eq. 16:

$$\boldsymbol{F} = \boldsymbol{F_4} \cdot \boldsymbol{F_5} \cdot \boldsymbol{F_1} \cdot \boldsymbol{F_3} \cdot \boldsymbol{F_2} \cdot \boldsymbol{F_3} \cdot \boldsymbol{F_1} \cdot \boldsymbol{F_5} \cdot \boldsymbol{F_4}$$

$$\boldsymbol{F_4} = \begin{bmatrix} 1 & j\frac{X_b}{2} \\ 0 & 1 \end{bmatrix}, \boldsymbol{F_5} = \begin{bmatrix} 1 & 0 \\ \frac{j}{X_a} & 1 \end{bmatrix} \quad , \quad (16)$$

where $\boldsymbol{F_4}\boldsymbol{F_5}$ is the transferring matrix of section A. For a periodic system, the relative field distribution of its periodic modes varies periodically, although the phase and amplitude may have a certain change. According to the criterion, the Eigen mode problem of the transferring matrix is solved, shown as Eq. 17:

$$\boldsymbol{F}\begin{bmatrix} V \\ V/Z_t \end{bmatrix} = e^{-j\Phi}e^{-A}\begin{bmatrix} V \\ V/Z_t \end{bmatrix} \quad , \quad (17)$$

where Φ is the periodic phase shift and A is the periodic amplitude attenuation factor , Z_t is the mode impedance on the axial cross section. There are two solutions, representing the periodic mode wave propagating along adverse directions, whose value is opposite to each other. For simplification, only properties of wave propagating along +z are discussed in the following content. The electron beam passes along z axis, thus the complex amplitude of E_z field along z axis is plotted in Fig. 3, including the phase variation and amplitude variation messages.

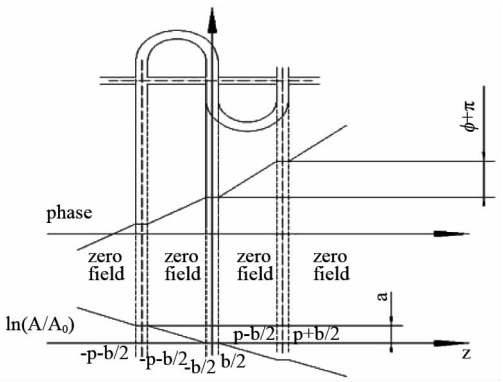

Fig. 3　The phase and amplitude of E_z field along z axis
图 3　纵向电场沿 z 轴的相位和幅度分布

Notice that in common area of beam and wave, the E_z field is unvaried along z. Since the normalized field between two adjacent common area is opposite, the periodic phase shift of E_z is $\Phi + \pi$.

The minimal positive period of FW along z axis is $2p$. Therefore, the E_z field along z axis can be seen as the superposition of infinite harmonics by Fourier decomposition, shown as Eq. 18:

$$E_z(z) = \sum_{-\infty}^{\infty} A_m e^{-j\frac{z}{2p}4m\pi} e^{-j\frac{2\Phi+2\pi}{2p}z} e^{-\frac{2A}{2p}z} \quad , \quad (18)$$

where m is the ordinal number of harmonics which can be $-\infty, \cdots, -3/2, -1, -1/2, 0, 1/2, 1, 3/2, \cdots, +\infty$. A_m is the complex amplitude of the m-harmonics at $z = 0$. The phase velocity and attenuation coefficient of harmonics could be written as Eq. 19:

$$v_{pm} = \omega p/(\Phi + \pi + 2m\pi), \alpha = A/p \quad . (19)$$

A_m can be solved, in consideration of the orthogonal characteristic of harmonics, shown in Eq. 20:

$$2pA_m = \int_{-p}^{p} E_z(z) e^{+j\frac{z}{p}2m\pi} e^{+j\frac{\Phi+\pi}{p}z} e^{+\frac{A}{p}z} \mathrm{d}z \quad . \quad (20)$$

According to E_z field demonstrated in Fig. 3, the A_m equals zero when m is half integer. When m is a integer, Eq. 20 is evolved to Eq. 21 by narrowing the integration interval to $[-b/2, b/2]$:

$$A_m = \frac{2E_0}{\Phi + \pi + 2m\pi - jA} - \sin\left(\frac{\Phi + \pi + 2m\pi - jAb}{p} \cdot \frac{b}{2}\right) \quad , \quad (21)$$

where E_0 is the complex amplitude of E_z field at $z = 0$. The relationship between E_0 and transmission power of the periodic TE_{10} mode is derived using the definition of mode impedance, shown as Eq. 22:

$$\frac{|E_0|^2}{P_z} = \frac{|Ve_0|^2}{\frac{1}{2}\mathrm{Re}(V^* \cdot \frac{V}{Z_t})} = \frac{2e_0^2}{\mathrm{Re}(\frac{1}{Z_t})}, e_0 = \sqrt{\frac{2}{ab}} \quad (22)$$

where e_0 is the scalar normalize electric field at the center of rectangular waveguide. The coupling impedance of harmonics is given according to Eq. 21, Eq. 22, demonstrated as Eq. 23:

$$K_m = \frac{|A_m|^2}{2\beta_m^2 P_z} = \frac{2b}{a} \cdot \frac{1}{\mathrm{Re}(\frac{1}{Z_t})} \cdot \frac{\left|\mathrm{Sa}\left(\frac{\Phi + \pi + 2m\pi - jA}{2}\frac{b}{p}\right)\right|^2}{(\Phi + \pi + 2m\pi)^2} \quad (23)$$

where S_a is the sampling function, m is integer number. The axial coupling impedance is zero for these harmonics with half integer m in ECM. The beam tunnel causes the field leaking into the zero-field-area shown in Fig. 3 and distorted the field distribution of TE_{10} mode near the aperture. Thus the axial impedance of harmonics should be modified as Eq. 24[11]:

$$K_{axis,m} = K_m / I_0^2(r_c \sqrt{(\frac{\omega}{v_p m})^2 - (\frac{\omega}{c})^2}) \quad (24)$$

The electron beam occupies certain space in the beam tunnel and the field enhances with its position offset from the axis. Therefore, the average impedance in cylindrical beam area is slightly larger than the axial impedance, shown in Eq. 25[5]:

$$K_{beam,m} = K_{axis,m}[I_0^2(r_m \sqrt{\beta_m^2 - (\frac{\omega}{c})^2}) - I_1^2(r_m \sqrt{\beta_m^2 - (\frac{\omega}{c})^2})] \quad (25)$$

3 Numerical Verification

For the analysis of the waveguide system with lossy wall, the ECM considering the loss effect in a self-consistent way described above can be more practical than previous loss-free system by letting the conductivity of metallic wall to a value obtained by Eq. 1 or experimental method in terahertz situation.

By calculating the Eigen mode of a 3-D numerical model loaded with periodic boundary conditions, the resonant frequency and field distribution can be gained. It should be emphasized that the FW periodic system has a minimal positive period (MPP) of $2p$ along z direction, shown in Fig. 4. If the perfect electric or magnetic boundary is launched at periodic position in beam tunnel shown in Fig. 4, the MPP of FW system can be seen as p along waveguide serpentine direction though the MPP of FW SWS. Based on this assumption, the compete $2p$ periodic solution can be pieced together by the solution of FW system of length of p, just as the above ECM and some numeric method[5]. In the below simulation, the whole $2p$ periodic FW system is adopted directly.

Then the material of the wall can be set for the quality factor of the resonant mode using perturbation method. According to definition of the quality factor, the

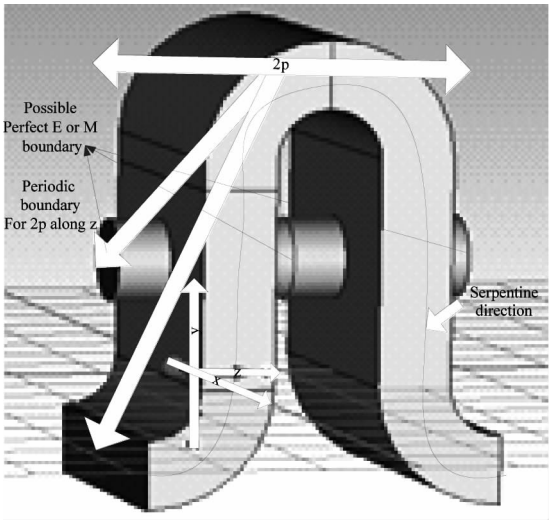

Fig. 4 3-D numerical model for FW SWS
图4 折叠波导慢波结构的三维数值模型

whole power loss on the ohm surface could be written as Eq. 26:

$$P_{loss} = 2\pi f W/Q \quad (26)$$

where W is the time-average energy stored in the cavity, Q is the quality factor calculated by numeric simulation. This solution amounts to calculate the periodic phase shift value, mode field distribution and quality factor at certain frequency. By sweeping the periodic phase shift value, the dispersive characteristics of FW SWS is demonstrated.

The parameters of SWS are set as the optimized results for 220 GHz FW BWO, shown as Table. 1.

Table 1 Parameters of the SWS for 220 GHz FW BWO
表1 220 GHz 折叠波导返波管的慢波线参数

a/mm	b/mm	l_0/mm	p/mm	r_c/mm	r_m/mm	m	σ $\Omega^{-1}m^{-1}$
0.73	0.16	0.53	0.39	0.095	0.08	-2	5.8×10^7

Periodic boundary conditions are applied in z-direction. If the periodic boundary conditions with phase shift 2Φ are launched in this numerical model, there will be many Eigen modes to be solved. Only transverse TE_{10} mode with consecutive phase shift 2Φ along serpentine direction is used to be further analyzed. It is assumed that the m-harmonic possesses consecutive phase shift of $2\Phi + 2\pi + 4m\pi$ along z axis, where $m = -\infty, \cdots, -3/2, -1, -1/2, 0, 1/2, 1, \cdots$. According to the simulation results of the resonant frequency f, E_z distribution along z and the transmission power P_z, Eqs 20, 21, 23 and 24 could be adjusted to approach the phase velocity and coupling impedance of the harmonic of the periodic TE_{10} mode. The loss effect is considered using the perturbed power dissipation caused by the surface current calculated in loss free situation demonstrated as Eq. 27:

$$v_{pm} = \frac{2\pi f p}{\Phi + \pi + 2m\pi}$$

$$A_m(r,\theta) = \frac{1}{2p}\int_{-p}^{p} E_z(r,\theta,z) e^{+j\frac{z}{p}2m\pi} e^{+j\frac{\Phi+\pi}{p}z} \mathrm{d}z$$

$$K_m(r,\theta) = \frac{|A_m|^2}{2(\Phi + \pi + 2m\pi)^2 P_z}$$

$$K_{aver}(r_m) = \frac{\int_0^m r\mathrm{d}r \int_0^{2\pi} K_m(r,\theta)\,\mathrm{d}\theta}{\pi r_m^2}$$

$$\alpha = A/p = -\frac{1}{4p}\ln\left(1 - \frac{P_{loss}}{P_z}\right) = \frac{1}{4p}\ln\left(1 - \frac{P_z Q}{2\pi f W}\right) \quad (27)$$

Notice that the space harmonics with m of half integer number emerges. It can be proved these categories of harmonics have exactly zero axial coupling impedance when the perfect electric or magnetic boundary is launched at periodic position in beam tunnel shown in Fig. 4. In our numeric model, the axial coupling impedance is much weaker than its adjacent space harmonic with integer m. That is why these space harmonics are often neglected in conventional analysis. The distribution of coupling impedance of space harmonics with $m = -2, -1, 0, -0.5$ in FW system around 220 GHz is demonstrated in Fig. 5.

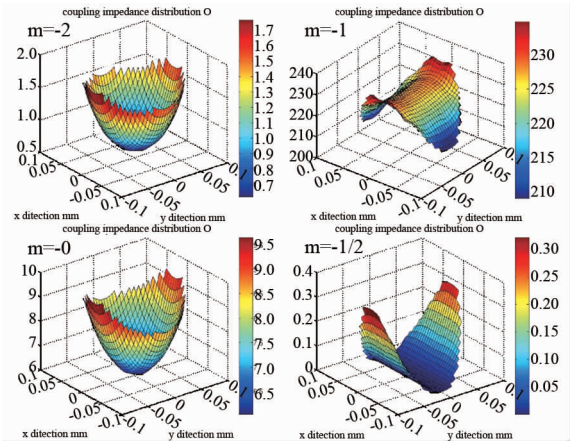

Fig. 5　The distribution of coupling impedance of some space harmonics in FW system at 220 GHz
图 5　220 GHz 折叠波导系统中一些空间谐波的耦合阻抗分布情况

The result of the numeric model is obtained after mesh convergence analysis, in which the total number of the mesh cells is about 1 million. Large numeric calculations show that not every space harmonic has a proximately round symmetric distribution of coupling impedance and the space harmonics with a half integer number always have weak axial coupling impedance. Nevertheless, the average coupling impedance of an ideal round electron beam calculated as Eq. 27 is always a considerable value for all space harmonics. For a normal size of FW device operating between 100 ~ 800 GHz, the synchronized voltage for space harmonic with $m = -2$ and $m = 0$ is about several tens of kilovolt, which can be conveniently realized by a conventional compact thermo electron gun. Therefore, most FW TWT selects harmonic with $m = 0$ as operating harmonic and FW BWO selects harmonic with $m = -2$. The phase velocity and the attenuation coefficient of backward harmonic wave were calculated by numerical method and equivalent circuit theory is plotted in Fig. 6(a). And the axial coupling impedance and average coupling impedance were also calculated by these two methods, shown in Fig. 6(b).

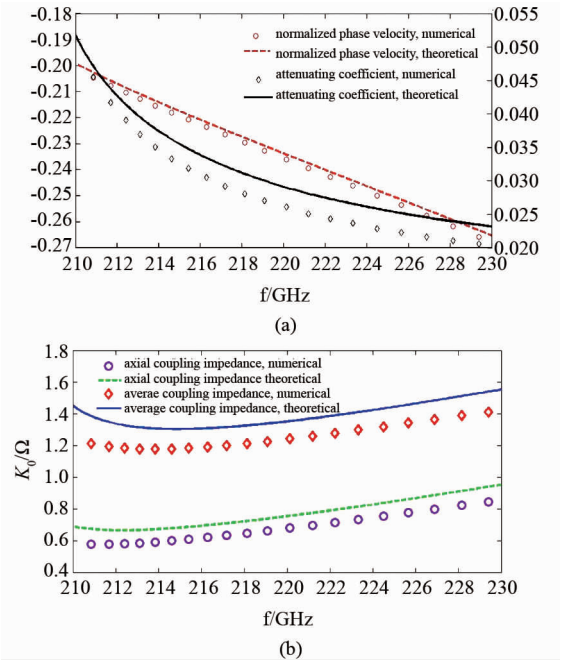

Fig. 6　phase velocity, attenuation coefficient and coupling impedance calculated by two method
图 6　两种方法计算的相速度,衰减系数和耦合阻抗

For 220 GHz FW BWO, backward wave with harmonic number of -2 is adopted as the synchronized harmonics for which the comparison is put forward.

The discrepancies of phase velocity, the attenuating coefficient and the axial coupling impedance calculated by two methods are less than 1%, 10%, and 15%, respectively.

Further calculation shows that, the model error of the equivalent circuits increases when the higher harmonic number wave is under analysis. For forward harmonic wave of $m = 0$ used as synchronizing wave in FW traveling wave amplifier, the discrepancy of phase velocity, coupling impedance and attenuating factor calculated by these two methods could be confined to 0.5%, 10% and 10% respectively.

It should be emphasized that loss-free FW SWS almost has the same dispersion characteristic and coupling impedance as the lossy system, whose discrepancies are respectively less than 0.01% and 0.1% according to analytical calculation. The key point in our self-consistent model is to calculate the attenuating factor, which is neglected in loss-free model. This also tells us the perturbation method adopted in numeric simulation is reasonable.

Using numerical model, dispersion characteristics of periodic TE_{20} mode can also be calculated. Due to its weak axial E_z field, TE_{20} mode can hardly interact with round electron beam efficiently. The dispersion properties of TE_{10} mode and TE_{20} mode are shown in Fig. 7 to give a comprehensive understanding.

Both linear and nonlinear model of 1-D particle-mi-

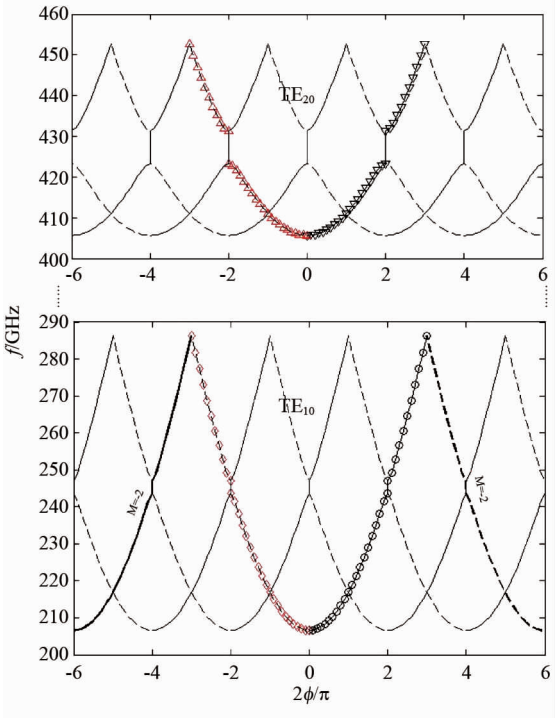

Fig. 7 TE_{10} and TE_{20} modes in FW periodic structure
图 7 折叠波导周期结构中的 TE_{10} 和 TE_{20} 模式

crowave interaction was established to design the 220 GHz FW BWO[12], with cold wave properties calculated by the equivalent circuit theory described in Part three. Both the loss-free SWS and the lossy SWS with the same dimension demonstrated in Table. 1 was used to calculate the backward wave oscillation properties with the same electron beam injection condition. The PIC model with the consideration of the lossy wall was also established with commercial computer code to give a comparison, shown in Fig. 8. The axis magnetic field is about 50 times Brillouin value to confine the beam a 1-D like movement. The effective conductivity was calculated as Eq. 1, where copper metallic wall with surface roughness of 0.2 mm is studied. The mesh convergence analysis shows that the numeric result is convincible, where several millions of mesh grids are tested. The investigation result is shown in Fig. 9.

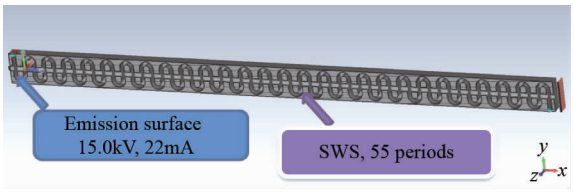

Fig. 8 The PIC model of FW BWO
图 8 折叠波导返波管中的 PIC 模型

From the comparison data, it is proved that the backward wave oscillation property is obviously different whether the ohm loss in the waveguide wall is considered or not. And the data calculated from the equivalent circuit theory satisfies the PIC calculation well when the same lossy wall condition is used. That is exciting evidence that our modified equivalent circuit theory in consideration of lossy wall gives a good description of the cold wave properties of FW BWO.

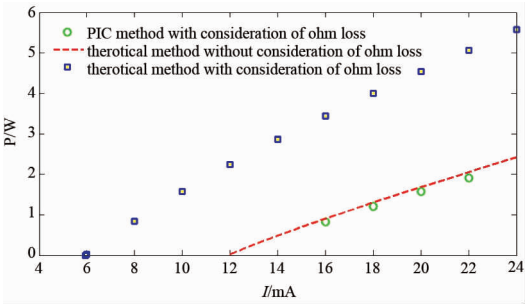

Fig. 9 The oscillation properties with or without ohm loss
图 9 考虑和不考虑欧姆损耗的微波振荡特性

4 Conclusion

The dispersion and attenuating properties of the 220 GHz FW SWS was discussed both in theoretical and numerical method. As a self-consistent model in consideration of lossy wall, the modified equivalent circuit theory fits numerical simulation well.

The accuracy of the loss calculation greatly depends on the accuracy of value of the effective conductivity, which would be better gained through experimental method[13]. Since the skin depth of microwave into copper is about 0.14 μm, the FW SWS with surface roughness of 0.2 μm seems the limitation criterion of surface finish, although the tested effective conductivity is not so bad as the theoretical prediction.

Traditional machining work including milling, lathing, lapping and electric discharging operation can only guarantee the surface roughness of 0.1μm with high precision. To improve the surface finish, UV-LIGA is considered to control the roughness to dozens of nanometers.

The 220 GHz FW BWO have been designed and the components of proto-type tube are under machining.

References

[1] SIEGEL P H. Terahertz technology [J]. *IEEE tran. Microw. Theory Tech*, 2002, **5**(3):910-928.
[2] GALLERANO G P, BIEDRON S. Overview of terahertz radiation sources[C]. *Proc. of the* 2004 *FEL conference*, Trieste, Italy, 2004.
[3] BHATTACHARIJEE S, BOOSKE J H, KORY C L, *et al.* Folded waveguide traveling-wave tube sources for terahertz radiation [J]. *IEEE. trans. on. plas. Sci*, 2004, **32**(3):1002-1014.
[4] JUN Cai. Study of W-band folded waveguide slow wave structure[D]. Doctorate Dissertation in Shandong University, 2006.
[5] BOOSKE J H, CONVERSE M C, KORY C L, *et al.* Accurate parametric modeling of folded waveguide circuits for millimeter-wave traveling wave tubes[J]. *IEEE. Trans. on Plasm. Sci*, 2005, **52**(5):461-462.
[6] HFSS12.0 online help[R]. ANSOFT Corporation, 2009.
[7] ZHANG Ke-Qian, LI De-Jie. Electromagnetic Theory For Microwaves and Optoelectronics[M]. Beijing: Publishing House of Electronics Industry, 2001, 99-101.
[8] KIRLEY M P, BOOSKE J H. Increased resistance of rough copper

surfaces at terahertz frequencies: 15th IEEE *Int. vacc. elec. conf*, *Monterey*, *California*, 2014[C]. US: Institute of Electrical and Electronics Engineering, 2014.

[9] HUANG Hong-Jia. *Principle of Microwaves*[M]. Beijing: Publishing House of Science(黄宏嘉, **微波原理**, 北京: 科学出版社), 1964.

[10] MARCUVITZ N. *Waveguide handbook*[R]. Stevenage, U. K.: Peregrinus, 1986.

[11] Hutter R G E. *Beam and Wave Electronics in Microwave Tubes*[M]. New York: Van Nostrand, 1960.

[12] CAI Jin-Chi, HU Lin-Lin, MA Guo-Wu, *et al*. Theoretical models for designing a 220-GHz folded waveguide backward wave oscillator[J]. *Chin. Phys. B*. 2015, **24**(6): 060701.

[13] KIRLEY M P, BOOSKE J H, Study of the effect of surface roughness and skin depth on the conductivity of metals at 650GHz[C]. 13th IEEE *Int. vacc. elec. Conf.*, *Monterey*, *California*, 2012. US: Institue of Electrical and Electronics Engineering, 2012.